

Geomagnetic activity signatures in wintertime stratosphere wind, temperature, and wave response

A. Seppälä,¹ H. Lu,² M. A. Clilverd,² and C. J. Rodger³

Received 1 October 2012; revised 30 January 2013; accepted 31 January 2013; published 12 March 2013.

[1] We analyzed ERA-40 and ERA Interim meteorological re-analysis data for signatures of geomagnetic activity in zonal mean zonal wind, temperature, and Eliassen-Palm flux in the Northern Hemisphere extended winter (November–March). We found that for high geomagnetic activity levels, the stratospheric polar vortex becomes stronger in late winter, with more planetary waves being refracted equatorward. The statistically significant signals first appear in December and continue until March, with poleward propagation of the signals with time, even though some uncertainty remains due to the limited amount of data available (~50 years). Our results also indicated that the geomagnetic effect on planetary wave propagation has a tendency to take place when the stratosphere background flow is relatively stable or when the polar vortex is stronger and less disturbed in early winter. These conditions typically occur during high solar irradiance cycle conditions or westerly quasi-biennial oscillation conditions.

Citation: Seppälä, A., H. Lu, M. A. Clilverd, and C. J. Rodger (2013), Geomagnetic activity signatures in wintertime stratosphere wind, temperature, and wave response, *J. Geophys. Res. Atmos.*, 118, 2169–2183, doi:10.1002/jgrd.50236.

1. Introduction

[2] Solar activity in the form of solar storms and geomagnetic activity (henceforth we referred to this type of activity as geomagnetic activity to distinguish from solar cycle UV and solar irradiance variations) has great potential to affect the Earth's middle and upper atmosphere. It is now well known that ionization from particle precipitation during geomagnetic activity provides a direct chemical coupling mechanism from the Sun to the atmosphere via the production of NO_x and HO_x, constituents which are important to middle atmosphere ozone balance [e.g., Randall *et al.*, 2005; Seppälä *et al.*, 2007; Verronen *et al.*, 2011; Andersson *et al.*, 2012]. Geomagnetic activity driven signatures have been found in various meteorological and climate records [e.g., Lu *et al.*, 2008a; Seppälä *et al.*, 2009; Lockwood *et al.*, 2010], but it has remained unclear which mechanism or mechanisms would be responsible for communicating geomagnetic activity variations to climate variables such as stratospheric and tropospheric temperatures.

[3] Rozanov *et al.* [2005] and Baumgaertner *et al.* [2011] investigated the top-down link from mesospheric NO_x production with independent climate models, but while their individual model results predicted significant perturbations in stratospheric and tropospheric temperatures during

polar winter, their analysis did not conclusively determine the underlying cause that led to the downward descent of the signals. Rozanov *et al.* [2005] included a low intensity, continuous electron precipitation forcing in their model, providing a source for NO_x (energetic particle precipitation produced NO_x, EPP-NO_x) in the middle atmosphere. The predicted EPP-NO_x enhancements led to up to 30% annual decrease in polar stratospheric ozone, accompanied by significant polar stratospheric temperature reductions. Furthermore, the model results also showed changes in surface air temperatures, but the mechanisms driving the surface level changes remained unclear. In the study of Baumgaertner *et al.* [2011], the model experiment included an A_p index-driven EPP-NO_x source at the mesospheric upper boundary (0.01 hPa). They then used a chemistry general circulation model to simulate surface temperature response to geomagnetic activity variations by realistically varying the A_p index to further explore the mechanisms leading to the temperature responses reported earlier by Rozanov *et al.* [2005]. The A_p-driven NO_x parameterization that they used in their model had previously proved to be realistic and in a good agreement with observations [Baumgaertner *et al.*, 2009], concurring well with earlier observations of the relationship between polar middle atmosphere NO_x concentrations and the variation in geomagnetic activity and particle precipitation [Siskind *et al.*, 2000; Randall *et al.*, 2007; Seppälä *et al.*, 2007; Sinnhuber *et al.*, 2011]. Baumgaertner *et al.* [2011] showed the temperature response from 0.01 hPa to 1000 hPa (mesopause to surface) when the model was forced with the A_p-controlled EPP-NO_x (their Figure 9). They saw a positive temperature response in the Northern Hemisphere (NH) polar winter (December–February mean) upper stratosphere-mesosphere, while lower altitudes (5 hPa to 110 hPa) showed cooling. Simultaneously, the model

¹Finnish Meteorological Institute, Helsinki, Finland.

²British Antarctic Survey, NERC, Cambridge, UK.

³Department of Physics, University of Otago, Dunedin, New Zealand.

Corresponding author: A. Seppälä, Finnish Meteorological Institute, Helsinki, Finland. (annika.seppala@fmi.fi)

©2013. American Geophysical Union. All Rights Reserved.
2169-897X/13/10.1002/jgrd.50236

results predicted stratospheric and mesospheric ozone reductions from the NO_x enhancements (their Figure 8).

[4] *Baumgaertner et al.* [2011] suggested that the temperature responses in the model could be a combination of a radiative response to the ozone reduction and a subsequent dynamical response to changes in the radiative balance. This type of process initiated by ozone reduction had previously been discussed by *Langematz et al.* [2003]. According to *Langematz et al.* [2003], reduced ozone levels at stratosphere–lower mesosphere altitudes during the polar winter [see also *Langematz*, 2000] lead to net radiative warming above the stratopause due to reduced long-wave radiative cooling: during polar winter, the terrestrial long-wave radiation processes are more effective than the solar-driven short-wave radiation processes which dominate in the sunlit atmosphere. These radiatively initiated changes in temperatures above the polar stratopause would affect both the meridional temperature gradient and planetary wave propagation patterns. During the winter, a reduction in the upward planetary wave forcing into the stratosphere would lead to a slowing down of the mean meridional circulation, which in turn would result in anomalous cooling of the polar stratosphere. Based on this, *Baumgaertner et al.* [2011] proposed that the lower stratospheric cooling signal they saw was a result of a dynamical response. They did not, however, analyze the wave propagation response from their EPP- NO_x model experiment results to verify this.

[5] Most recently, *Kvissel et al.* [2012] investigated the effects that EPP- NO_x might have on the springtime middle atmosphere through chemical-dynamical feedbacks using a chemistry-climate model. They suggested a new pathway involving stratospheric nitric acid, which could further amplify the EPP- NO_x indirect effect on dynamics beyond the winter season. They proposed that the modeled weakening of zonal-mean polar winds during the spring (April–May) arose from EPP- NO_x -driven zonal asymmetries in middle atmosphere ozone, affecting short-wave heating patterns.

[6] Looking at the zonal mean flow responses, *Lu et al.* [2008b] suggested that geomagnetic activity may induce significant variability in the NH stratospheric circulation extending down to the troposphere through vertical coupling via the Northern Annular Mode (NAM). They found significant correlations between geomagnetic activity and the winter NAM during high solar irradiance cycle conditions (solar maximum) and speculated that increased geomagnetic activity could lead to a strengthened polar vortex, reduced Brewer-Dobson circulation, and enhanced stratosphere-troposphere coupling. *Lu et al.* [2008b] suggested that the combined effect of high solar UV irradiance and enhanced geomagnetic activity could result in more planetary waves being refracted toward the equator, which would then lead to the strengthening of the polar vortex.

[7] Considering these previous studies together, they all seem to point toward wave-mean flow interaction as a key for linking geomagnetic forcing and dynamic responses in the stratosphere and troposphere. This provides us with a motivation to undertake the first analysis of changes in wave propagation and breaking in association with changes in geomagnetic forcing.

[8] In this paper, we examine the Northern Hemisphere stratospheric and tropospheric temperature (T), zonal

wind (U), and Eliassen-Palm (EP) fluxes using re-analysis data during high and low geomagnetic forcing to determine the full dynamical and wave forcing response. We focus on the dynamical processes taking place in the Northern wintertime (November–March) stratosphere. In order to verify the dynamical mechanism discussed above for the case of geomagnetic activity, our results will need to show that for elevated geomagnetic activity, there is (1) reduction of upward wave propagation into the stratosphere with more waves refracting toward the equator, (2) strengthening of the polar vortex, and (3) cooling of the polar stratosphere.

[9] Analogously to the methods previously used, e.g., by *Lu et al.* [2008b], we will also further separate the data according to high and low solar irradiance levels (referred to as HS and LS, respectively) and westerly and easterly quasi-biennial oscillation (wQBO and eQBO) to examine the potential HS and LS, and QBO conditioning of the atmospheric response to geomagnetic forcing.

2. Data and Method

[10] The ERA-40 data set, described by *Uppala et al.* [2005], is a re-analysis of meteorological observations extending from September 1957 to August 2002. To extend the data further, we use the ERA Interim data from 1989 to 2008. The Interim data itself is at the time of writing available from 1979 onward, but for consistency with all data sets used in this study, we will utilize it for the period 1989–2008. Here we use all NH ERA-40 and ERA Interim data from 1957 to 2008, switching from ERA-40 data to Interim data in January 1989. Henceforth, we will refer to this blended data set as the ERA data. Because of the previous, relatively extensive use of the ERA data for studies on dynamical variability taking place in the atmosphere, the data set is suitable to examine the potential geomagnetic forcing impacts on large-scale stratospheric and tropospheric dynamics. The use of an established re-analysis data set like the ERA data also allows comparison of both magnitude and patterns with previous studies using the same data set. We note that there are potential temporal discontinuities in some variables when moving from the ERA-40 data to the ERA Interim data in 1988–1989. However, when performing the analysis using ERA-40 data alone, similar results were obtained.

[11] For the mean state variables, we analyze monthly mean zonal mean temperatures (T [K]) and zonal mean zonal winds (U [m/s]) from the ERA data. We use monthly mean EP fluxes provided by the Alfred-Wegener Institute (calculated from the ERA data according to *Andrews et al.* [1987]) and available from 1957 to 2008. As for the temperature and zonal wind data, we switched from ERA-40 to Interim in January 1989 for the EP flux data. EP fluxes are commonly used as a diagnostic tool for wave interaction with the mean flow [*Holton et al.*, 1995]. The flux is formed by two components: horizontal and vertical. By their definition [*Palmer*, 1981], the horizontal component is dominated by the momentum flux and the vertical by the eddy heat flux. The analysis of the meteorological data is done for the NH months from November to March, covering the extended winter period.

[12] At first we will analyze all the ERA data for geomagnetic forcing signals. We will refer to this as the All

SC group (All Solar Cycle). After this, we will examine responses to geomagnetic forcing during prevailing high or low solar irradiance forcing separately by grouping the data according to the solar irradiance cycle. Later, we apply the same analysis for data grouped according to the phases of the stratospheric quasi-biennial oscillation (QBO). The same method for dividing the data into high and low geomagnetic forcing cases, as described below, will be used throughout this paper. For the geomagnetic forcing, we divide the data into high geomagnetic activity (HA_p) and low geomagnetic activity (LA_p) years using the widely available geomagnetic activity index A_p (acquired from the National Geophysical Data Center, NGDC, <http://spidr.ngdc.noaa.gov/spidr>). The use of the A_p index allows us to utilize the full length of the ERA period with no data gaps and thus allows us to establish statistical significance. For our monthly analysis, we use a moving window for the A_p index to take into account any geomagnetic forcing of the upper atmosphere (mesosphere-thermosphere) prior to the month under investigation, as descent of anomalies from higher altitudes may take months to reach the stratosphere [Seppälä et al., 2007; Randall et al., 2005]. The window starts in October, when the dynamically active period starts in the NH [see, e.g., Cohen et al., 2002], and extends to the month under investigation (i.e., October–November, October–December, and October–January). For February and March, we will use the October–January window as any impacts from geomagnetic forcing on the atmosphere after January are less likely to result in a long-term effect [see, e.g., Salmi et al., 2011]. Thus, in February and March, we focus on following the propagation of any signals initiated during October–January. For each window (October–November, October–December, October–January), we calculate the median normalized A_p index for 1957–2008. The median normalized A_p is calculated as $(A_p - \text{median}(A_p))/\sigma(A_p)$, where $\sigma(A_p)$ is the standard deviation of the A_p index data set. We define cases where the normalized $A_p > 0.1$ as high geomagnetic activity and cases with $A_p < -0.1$ as low geomagnetic activity and refer to these cases as HA_p and LA_p , respectively. The years for each month in the HA_p and LA_p cases are listed in Table 1.

[13] In the second part, we further divide the ERA data into high and low solar irradiance cycles. This will allow us to assess potential solar irradiance level preconditioning of the atmosphere for the geomagnetic forcing effects. To estimate the solar irradiance cycle phase, we use solar radio flux ($F_{10.7}$ [10^{-22} W m $^{-2}$ Hz $^{-1}$]) data from the National Geophysical Data Center (NGDC, <http://spidr.ngdc.noaa.gov/spidr>). We separate the data into High Solar irradiance (HS) and Low Solar irradiance (LS) cycle phases following the same approach as for the A_p . For the solar irradiance cycle, we use a median normalized $F_{10.7}$ with a moving 6 month window and define HS as months where the normalized $F_{10.7} > 0.1$ and LS as $F_{10.7} < -0.1$. We then find the HA_p and LA_p cases described above in the HS and LS groups, giving us HS- HA_p & HS- LA_p and LS- HA_p & LS- LA_p . The years in each group are given in Table 2. Figure 1 presents, as an example, how the observed Solar Irradiance cycle ($F_{10.7}$) and the geomagnetic activity (A_p) varied for the ERA period Januaries. As the figure suggests, the correlation between the geomagnetic forcing and

Table 1. HA_p and LA_p Years for Each Month of Analysis for the All SC (All Solar Cycle)

Month	HA_p	LA_p
Nov	1959 <u>1960</u> 1962	1958 1964 <u>1965</u>
	<u>1963</u> <u>1968</u> 1973	1966 1967 1969
	1974 1975 <u>1981</u>	<u>1970</u> <u>1971</u> 1976
	1982 1983 1984	<u>1977</u> 1979 1986
	<u>1985</u> <u>1987</u> 1989	1988 1990 1995
	1991 1992 1993	1996 1997 2005
	1994 <u>1998</u> 1999	<u>2006</u> 2007 2008
	2000 2001 <u>2002</u>	
	<u>2003</u> <u>2004</u>	
Dec	1959 <u>1960</u> 1962	1964 <u>1965</u> 1966
	<u>1968</u> 1973 1974	1967 1969 <u>1970</u>
	1975 <u>1981</u> 1982	<u>1971</u> 1972 1976
	1983 1984 <u>1985</u>	<u>1977</u> 1979 1986
	1989 1991 1992	<u>1987</u> 1990 1995
	1993 1994 1999	1996 1997 <u>1998</u>
	2000 2001 <u>2002</u>	2005 <u>2006</u> 2007
	<u>2003</u> <u>2004</u>	2008
Jan–Mar	<u>1958</u> <u>1960</u> 1961	1962 1964 <u>1965</u>
	<u>1963</u> 1974 1975	1966 1967 <u>1968</u>
	1976 1979 1982	1969 <u>1970</u> <u>1971</u>
	1983 1984 <u>1985</u>	1972 <u>1977</u> 1978
	1986 1989 1990	1980 <u>1981</u> <u>1987</u>
	1992 1993 1994	1991 1996 1997
	1995 2000 <u>2003</u>	<u>1998</u> 1999 2001
	<u>2004</u> 2005	<u>2006</u> 2007 2008

Years when a midwinter SSW occurred have been underlined.

the $F_{10.7}$ solar irradiance proxy is relatively low. For the months of January, the correlation coefficient $r(A_p, F_{10.7})$ is 0.24, while for all months of the ERA period, it is 0.39. This allows for a good representation of both HA_p and LA_p cases inside the HS and LS groups.

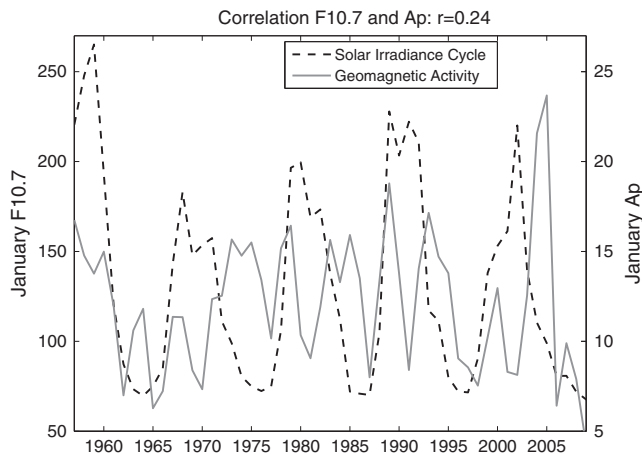
[14] We will present the results for T, U, and the EP flux as anomalies (deviation from the whole data series mean which we from now on refer to as climatology, i.e., HA_p -Climatology, LA_p -Climatology), or as HA_p - LA_p composite differences. All results are presented as zonal means. As a statistical test, we use the Student's t test, with 90%, 95%, and 99.5% significance levels shown for T and U and 90% and 95% levels shown for EP flux divergence in the figures. We also tested the robustness of the t test results by applying a random permutation test with 10,000 repetitions to part of the analysis. The results from the random permutation test, which are discussed in more detail in the Appendix, were able to confirm the t test results, thus adding confidence to the chosen method. It is important to keep in mind that statistical significance alone does not indicate causality. Rather, when examining the responses for the different variables, we have aimed to assess if the signals are dynamically consistent.

[15] It is known that atmospheric temperature distributions and dynamics are affected by atmospheric oscillation modes such as the ENSO (El Niño-Southern Oscillation) as well as major volcanic eruptions and the extreme dynamical conditions occurring during SSW (Sudden Stratospheric Warming) events. We will assess and discuss the potential effects of these on our results.

Table 2. HA_p and LA_p Years for Each Month of Analysis for the HS (High Solar Irradiance) and LS (Low Solar Irradiance) Groups, SSW Years Included

Month	HS- HA_p	HS- LA_p	LS- HA_p	LS- LA_p
Nov	1959 1960 1968 1981 1982 1989 1991 1992 1998 1999 2000 2001 2002 2003	1958 1967 1969 1970 1979 1988 1990	1962 1963 1973 1974 1975 1984 1985 1987 1993 1994 2004	1964 1965 1966 1976 1977 1986 1995 1996 1997 2005 2006 2007 2008
Dec	1959 1960 1968 1981 1982 1989 1991 1992 1999 2000 2001 2002 2003	1967 1969 1970 1979 1990 1998	1962 1973 1974 1975 1984 1985 1993 1994 2004	1964 1965 1966 1976 1977 1986 1987 1995 1996 1997 2005 2006 2007 2008
Jan–Mar	1958 1960 1961 1979 1982 1983 1989 1990 1992 1993 2000 2003 2004	1968 1969 1970 1971 1980 1981 1991 1999 2001	1963 1974 1975 1976 1985 1986 1994 1995 2005	1962 1964 1965 1966 1977 1978 1987 1996 1997 1998 2006 2007 2008

SSW years identified in Table 1.

**Figure 1.** Solar irradiance cycle progression ($F_{10.7}$) and geomagnetic activity (A_p index) for 1958–2008. Values are January monthly means. The $F_{10.7}$ radio flux units are [$10^{-22} \text{ W m}^{-2} \text{ Hz}^{-1}$]. The A_p index is dimensionless.

3. Results

3.1. Geomagnetic Signals in Dynamical Parameters

[16] In the first part of our study, we will focus on results from analysis where data from winters during which a mid-winter Sudden Stratospheric Warming (SSW) occurred [see Charlton and Polvani, 2007; Manney *et al.*, 2009] were omitted. While this does reduce the data set somewhat, it does not affect the overall U, T, and EP patterns, but in most cases leads to an improvement of the statistical significance of the results. This suggests that the stability of the polar atmosphere is important in observing the coupling from geomagnetic forcing to dynamical parameters. Similar results have been obtained by Seppälä *et al.* [2009] and Lu *et al.* [2008a]. The excluded SSW cases have been identified with underlining in Table 1. In the following discussion, we will mainly focus on those results that are found to be statistically significant. In order to enable a comparison between geomagnetic induced anomalies, i.e., deviation from climatology, Figure 2 shows the monthly U, T, and EP flux climatology values (ERA monthly means)

for the period 1957–2008. Each row corresponds to the calendar month shown on the left. The pressure levels shown are 1–1000 hPa, and the latitude range is 20°N – 90°N , these are used for all figures.

[17] Figure 3 shows the results for the All SC group. The three leftmost columns present the high geomagnetic activity (HA_p) anomalies for U, T, and EP flux and EP flux divergence, and the three rightmost columns the low geomagnetic activity (LA_p) anomalies for the same variables. For U and T, the 90%, 95%, and 99.5% significance levels are shown with continuous coloring and additional hatched and crossed shading, respectively. For the HA_p case, significant anomalies in both zonal mean zonal winds and temperatures are clearly observed from January to March, with U anomalies occurring in the stratosphere as early as December. The U anomalies are marked by enhanced zonal winds poleward of 40°N and reduced equatorward of 40°N . This signal extends from 1000 hPa to the upper stratosphere in January. As the winter progresses from February to March, the center of the U anomalies appears to shift poleward and downward with time. The HA_p zonal mean temperature anomalies start with a positive anomaly of up to 6 K in the polar upper stratosphere in January and a negative anomaly (up to -4 K) around 100 hPa. The positive and negative anomalies are mainly confined to the polar region and appear to descend, with the positive anomaly reaching the 30 hPa level at high latitudes in March and the negative anomaly descending to 200 hPa by February.

[18] The third column portrays the HA_p wave forcing response, i.e., the EP results. The EP flux (arrows) is used to show the direction of wave propagation [Palmer, 1981]. The EP flux divergence (contours) visualizes the wave forcing effect on zonal flow acceleration or deceleration: positive values (divergence, red) correspond to zonal flow acceleration and negative values (convergence, blue) to deceleration. The 90% and 95% significance levels for the EP flux divergence have been shaded in all figures by light and dark gray, respectively. The HA_p EP flux anomalies suggest that there is an overall enhancement in wave propagation or wave reflection toward the equator from about 60°N to 70°N in the stratosphere. Poleward of 60°N , the upward flux through the stratosphere is reduced from December to March. These

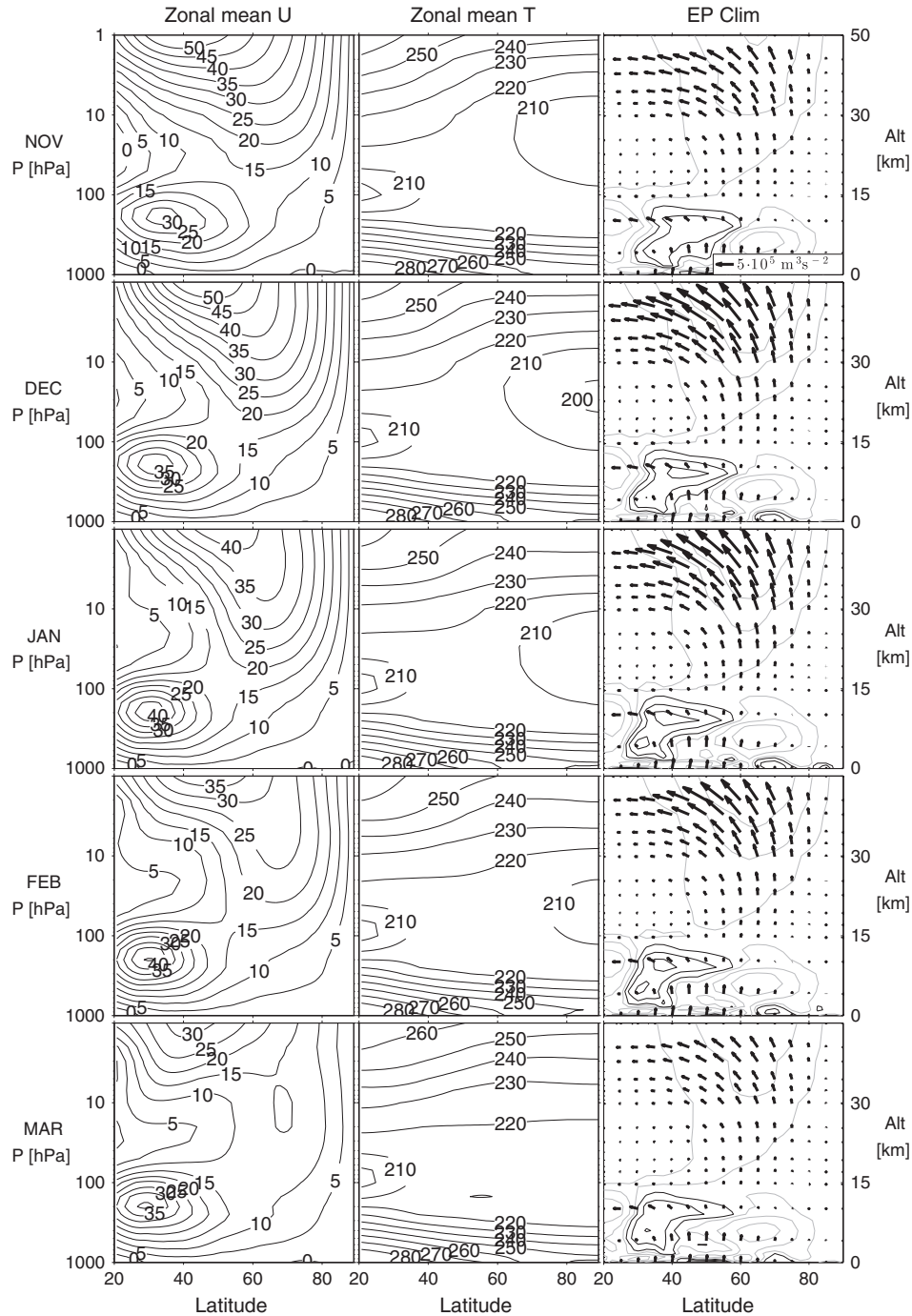


Figure 2. Monthly climatology for the zonal mean zonal wind (left), zonal mean temperature (middle), and EP flux (arrows) and EP flux divergence (contours) (right). Positive (negative) EP flux divergence is shown in black (gray). The values were calculated from the ERA-40 and ERA Interim data as described in the text. EP flux reference vector ($5 \times 10^6 \text{ m}^3 \text{ s}^{-2}$) is shown in the November panel. The EP fluxes were scaled according to [Bracegirdle, 2011]. The latitudes on the x axis are 20°N – 90°N , with pressure levels 1 to 1000 hPa on the y axis. The approximate altitude in kilometers is shown on the right.

wave anomalies start as early as December and continue throughout the winter until March, implying wave reflection toward the equator and away from the polar vortex, resulting in dynamically induced strengthening of the polar vortex.

[19] As a whole, the EP flux divergence results, where significant, suggest that from December onward the wave

divergence is acting to accelerate the stratospheric flow, first between about 60°N to 80°N and later, in January, around 40°N . The regions where the EP flux divergence anomalies are significant are very localized but well in agreement with the U anomalies. Below 100 hPa, the zonal mean flow is being accelerated north of 40°N starting in

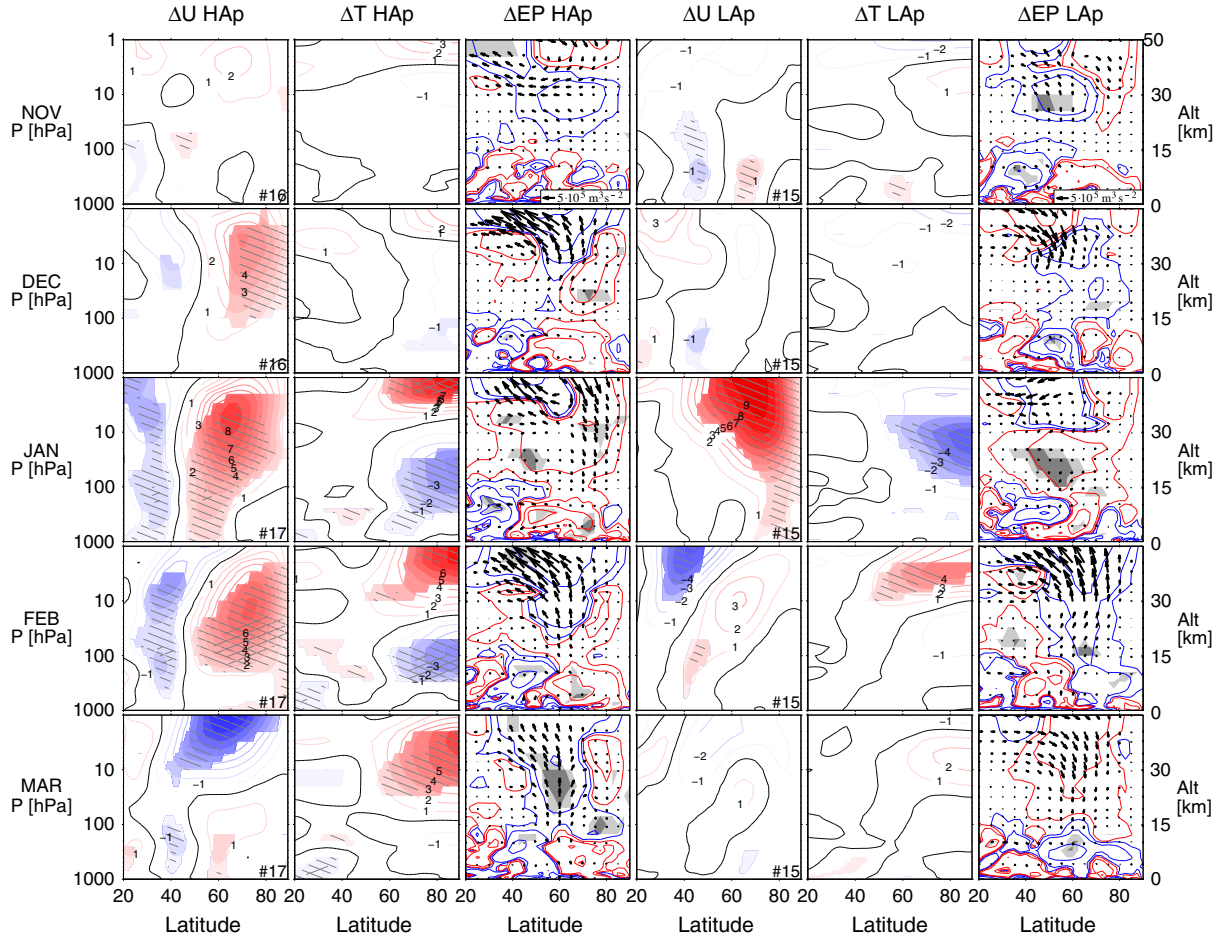


Figure 3. The monthly U, T, EP flux, and EP flux divergence anomalies for high geomagnetic forcing (HA_p–Climatology) on the left and for low geomagnetic forcing (LA_p–Climatology) on the right. The results are presented for latitudes 20°N–90°N and pressure levels 1–1000 hPa, with the approximate altitude shown on the right. All values that are statistically significant at $\geq 90\%$ level are colored for ΔU and ΔT with additional single-hatched shading for the $\geq 95\%$ level and cross-hatched shading for the $\geq 99.5\%$ level. For the ΔEP flux divergence, $\geq 90\%$ and $\geq 95\%$ levels are shown in light and dark shading, respectively. The number of HA_p and LA_p cases for each month is denoted with a # symbol in the bottom-right corner of the ΔU panel. The years are listed in Table 1. The EP fluxes were scaled according to Bracegirdle [2011], and the EP flux reference vector ($5 \times 10^5 \text{ m}^3 \text{ s}^{-2}$) is given in the top EP panels.

January. Simultaneously, wave convergence is working to decelerate the zonal flow in the troposphere equatorward of 40°N. This effect moves poleward until March, when the deceleration of the zonal wind extends all the way to the upper stratosphere.

[20] In the troposphere, this moving pattern in the EP flux convergence indicates a poleward movement of the tropospheric subtropical jet center, which is normally located around 30°N according to the climatology (Figure 2). This poleward movement of the tropospheric subtropical jet is consistent with the tropospheric response to stratospheric forcing suggested by Kushner and Polvani [2004]. However, it is important to keep in mind here that for our results the statistically significant areas in the HA_p troposphere EP flux convergence anomalies are very localized.

[21] In the LA_p case, shown in the three rightmost columns of Figure 3, weak zonal mean zonal wind anomalies start to occur in the troposphere around 45°N and 65°N

in November. These are accompanied by EP flux convergence between about 30°N and 50°N. By December, the wave convergence has shifted poleward to 40°N–60°N, in agreement with the simultaneous poleward movement of the negative wind anomaly. However, there is little signal in temperature, raising questions on the reliability of the signals seen in the zonal wind and EP flux as a result of dynamical response. Nevertheless, in December and January, the stratospheric EP flux anomaly shows waves directed more downward, which in the light of Figure 2 suggests a reduction in the upward wave propagation. As a result, in January both U and T anomalies show their largest variations, with positive wind anomalies being accompanied by negative temperature anomalies of up to -5 K around and below 10 hPa in the polar region. The signals in February and March are either rather weak or confined to the upper stratosphere. Some similarities in the LA_p and HA_p anomalies can be seen in January and February. For example, both show

cooling in the polar stratosphere in January and warming in the upper stratosphere in February. The overall patterns, however, are different, with the HA_p January temperatures also showing a highly significant ($>99.5\%$) warming region in the polar upper stratosphere and the cooling pattern below located in the lower stratosphere-upper troposphere region rather than the middle stratosphere. In February, an important difference is the cooling region ($>99.5\%$ significance) in the polar lower stratosphere-upper troposphere and in the troposphere around 20°N – 40°N , which is not present in the LA_p case.

[22] In comparison, the signals in the HA_p case show a consistent, although of varied statistical significance, positive EP flux divergence at the high-latitude troposphere and a negative divergence at the midlatitude subtropical region throughout December–March implying that less waves are getting into the high-latitude stratosphere and more waves are propagating toward the equator. This is not present under LA_p conditions. The poleward and downward movement of the signal is clearer in the HA_p case than in the LA_p case, suggesting that better stratosphere-troposphere coupling is taking place under HA_p than LA_p conditions.

3.2. Solar Cycle Phase Filtering

[23] Previous results of *Lu et al.* [2008b] suggested that solar irradiance levels may play a role in the effectiveness of coupling geomagnetic activity to the atmosphere through a modulation of stratospheric temperatures at low latitudes via changes in UV irradiance or effects arising from variations in the total solar irradiance through the solar cycle [Gray et al., 2010]. We examine this type of preconditioning of the atmosphere by dividing the data according to solar irradiance levels to High Solar irradiance (HS) and Low Solar irradiance (LS) groups as described in section 2. This is to test if a certain phase of the 11 year solar irradiance cycle, HS or LS, indeed provides better conditions for any geomagnetic forcing signals to be detected statistically. In the All SC group (Figure 3), we excluded data from winters during which a major SSW occurred during early to midwinter. In the HS and LS analyses, SSW years are included. The main reason for doing this is to have sufficient data samples: excluding the SSW years would leave fewer than 6–7 years in the HS- LA_p and LS- HA_p cases. We note that similar patterns were present when including or excluding the SSW years. The years for HS- HA_p , HS- LA_p and LS- HA_p , LS- LA_p are listed in Table 2.

[24] We now analyze the ($HA_p - LA_p$) differences for U, T, and EP flux. By taking the composite difference between the HA_p and the LA_p instead of the anomaly from the climatology, we avoid contaminating the signals with those arising from HS/LS solar irradiance forcing and can examine the modulating effect of solar irradiance on the geomagnetic signals of Figure 3 discussed in the previous section.

[25] Figure 4 presents the results for the HS case. As before, the rows top-down correspond to months from November to March. The columns from left to right present the ($HS-HA_p - HS-LA_p$) composite differences: ΔU , ΔT , and ΔEP . Similar to the All SC group discussed earlier, the most significant and persistent feature of ΔU is marked by a strengthening of the winds at the poleward side of the stratospheric polar vortex and a weakening of the winds at

the equatorward side of the vortex in January–March. The signal moves poleward and downward as the winter progresses. In agreement with *Lu et al.* [2008b], the signature in the zonal mean zonal wind projects positively on the Northern Annular Mode in both stratosphere and troposphere [Thompson and Wallace, 1998]. Note that the statistically significant regions in November and December should be regarded as less reliable than January–March signals, as only 6–7 years of data went in the November–December HS- LA_p groups (see Table 2).

[26] The most significant temperature response (ΔT) appears in the high-latitude stratosphere with warming signal in the upper stratosphere and cooling signal below. In the troposphere, persistent warming is observed from January to March at midlatitudes, with a slight downward movement with time. Again we note that the tropospheric warming and cooling signals in November–December might not be as reliable as the January–March signals.

[27] In terms of the geomagnetic effect on the wave propagation and breaking, there is an increase of EP flux from the troposphere to the stratosphere during early winter. As the winter progresses, more EP flux is directed toward the equator leading to strengthening of the wind at high latitudes and weakening of the wind at lower latitudes. The EP flux signal is accompanied by negative EP flux divergence in the upper stratosphere and positive EP flux divergence in the lower stratosphere, implying more wave breaking in the upper stratosphere and less wave breaking below under HS- HA_p conditions. These anomalous EP flux and EP flux divergence patterns appear to be dynamically consistent with the temperature anomalies in the high-latitude stratosphere.

[28] Figure 5 presents the corresponding results for the LS case. Unlike under HS conditions, for LS significant differences in wind, temperature, and wave activity occur in early winter instead of late winter. The early winter signal under LS conditions is characterized by an overall strengthening of the polar vortex in November and December associated with a cooler polar stratosphere and reduction of wave activity at high latitudes for LS- HA_p . Little signal is observed both in the mean state (U, T) and EP flux during January and February. For March, the blended ERA data results agree very well with the ERA-40 springtime (March–May) analysis of *Lu et al.* [2008a].

[29] At first, the wave response under LS conditions seems almost opposite to that under HS conditions. However, a closer examination suggests that the wave-mean flow interaction under HS conditions is mainly controlled by the horizontal EP flux during late winter, i.e., it is due to a modulation of the northward momentum flux [Palmer, 1981]. Contrarily, for the LS conditions the effect on the wave-mean flow interaction under HA_p is dominated by the vertical component of the EP flux, i.e., it is caused by a modulation of the eddy heat flux. For the earlier All SC case, both of these effects were taking place under HA_p conditions, with more waves being directed toward the equator at low latitudes and midlatitudes and less waves propagating from the troposphere to the stratosphere at high latitudes. Together these lead to strengthening of the polar vortex and, through that, to a positive modulation of the NAM [Baldwin and Dunkerton, 2001], linking to the positive NAM anomalies from geomagnetic and EPP forcing

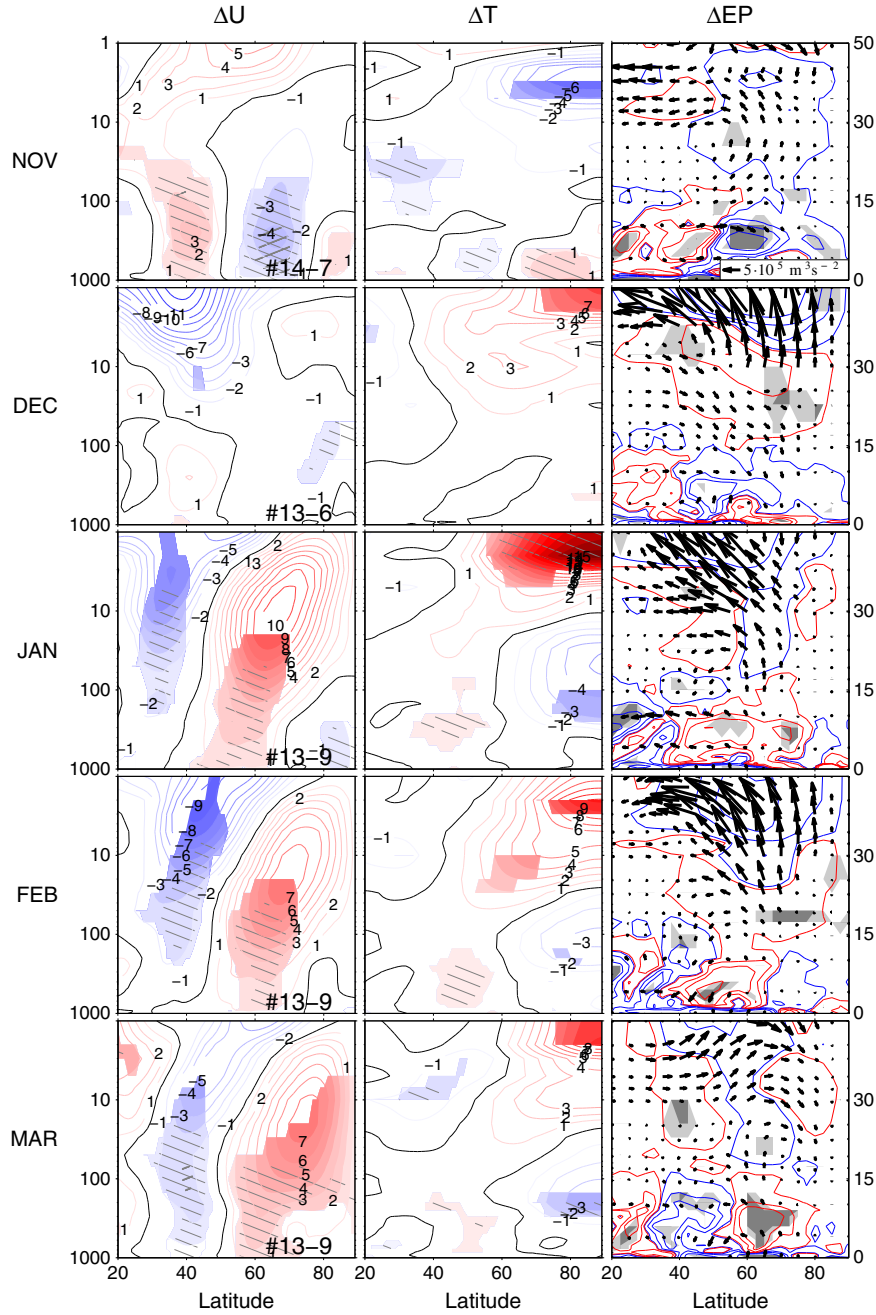


Figure 4. Monthly diagnostics for HS at latitudes 20°N–90°N and pressure levels 1–1000 hPa (approximate altitude [km] shown on right). Columns from left to right: zonal mean U difference ΔU , $HA_p - LA_p$; zonal mean T difference ΔT , $HA_p - LA_p$; and the difference in EP flux and divergence ΔEP , $HA_p - LA_p$. The $\geq 90\%$, $\geq 95\%$, and $\geq 99.5\%$ significance levels are indicated as in Figure 3, and the EP fluxes were scaled as before.

reported previously by, e.g., Seppälä *et al.* [2009] and Baumgaertner *et al.* [2011].

3.3. QBO Phase Filtering, ENSO, and Volcanic Eruptions

[30] Next we will examine the possibility that the geomagnetic signals discussed above may have been contaminated by other factors influencing atmospheric dynamics. We focus on those most likely to affect the area

of atmosphere under investigation: the stratospheric QBO, the ENSO, and major volcanic eruptions. We define the QBO phase from the normalized, de-seasonalized zonal wind from the ERA data near the equator [Lu *et al.*, 2009], with the normalized values of > 0.1 used to define the westerly phase (wQBO), and < -0.1 to define the easterly phase (eQBO). The number of wQBO and eQBO cases in the HA_p and LA_p groups in Figure 3 is presented in Table 3. Overall, both HA_p and LA_p have either fairly equal amounts

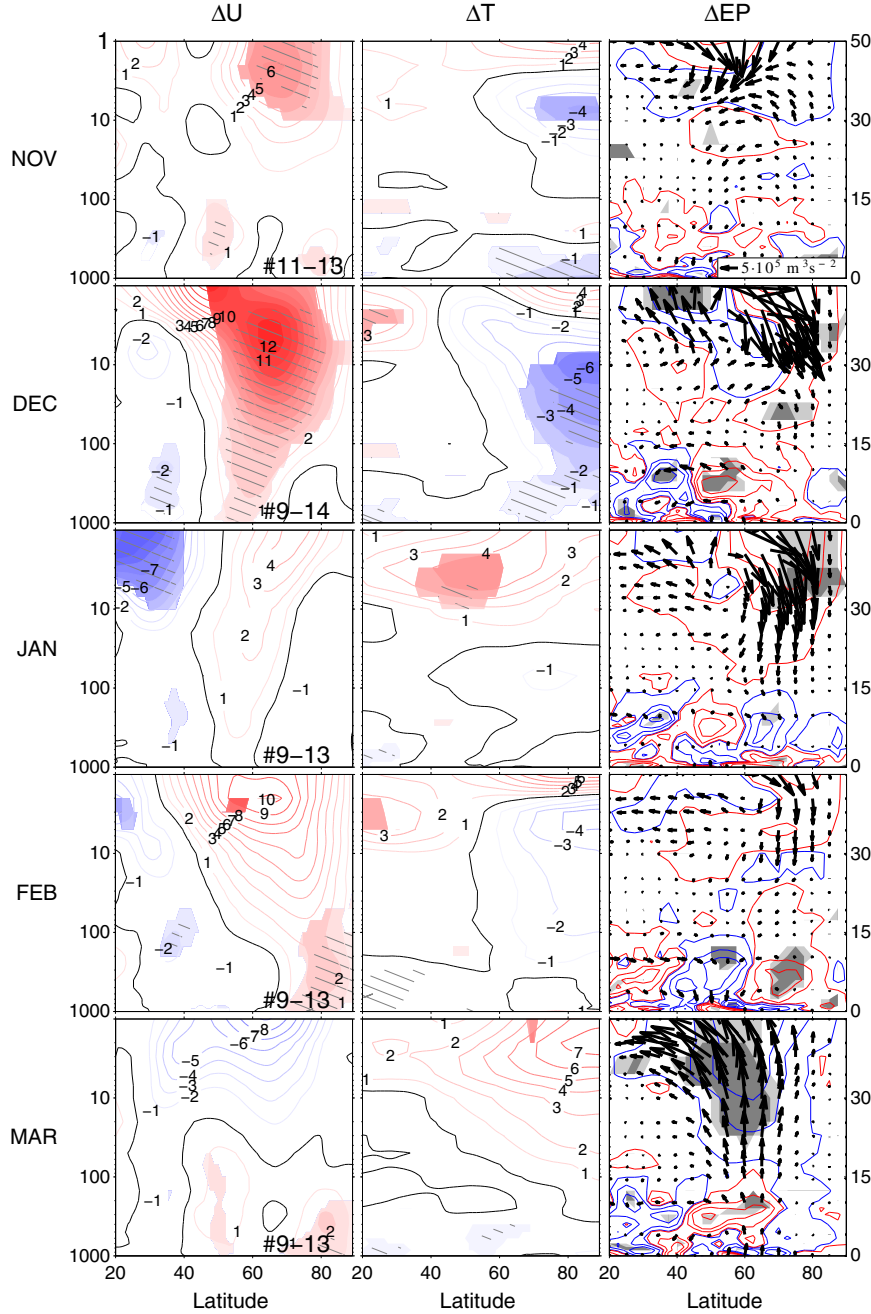


Figure 5. As in Figure 4 but for the LS case.

of wQBO and eQBO cases or slightly more wQBO cases. The balance of numbers of wQBO (and eQBO) between the HA_p and LA_p sets is fairly similar, for example for February there were 9 wQBO of all 17 HA_p cases, and 7 wQBO of all 15 LA_p cases (with 7 and 8 eQBO cases, respectively). Therefore, the HA_p group has a small tendency toward (i) eQBO during early winter and (ii) wQBO from January, while the opposite occurs for the LA_p group. As a whole, the HA_p – LA_p differences would have an eQBO bias during November and December and wQBO during January–March. According to Table 3, the largest bias should be in November. However, no clear geomagnetic signal was obtained in November (Figure 3), suggesting

that the QBO does not contribute significantly to the geomagnetic signal. Furthermore, it is known that the polar stratosphere during January–March is more disturbed under HS and wQBO conditions [Labitzke and Kunze, 2009], while our results indicate that the geomagnetic forcing signal obtained during the time is a strengthening of the polar vortex, with the signal arising mainly from HS conditions. Therefore, the QBO can be excluded as the driving factor for the signals at least in the All SC case (Figure 3) and under HS conditions (Figure 4).

[31] Although the QBO does not appear to cause the signals, it may precondition or modulate the mechanism linking geomagnetic activity to dynamical variables, as the solar

Table 3. Number of QBO Westerly and Easterly Cases for HA_p and LA_p

Month	QBO	HA_p	LA_p
Nov	wQBO	6	10
	eQBO	8	4
Dec	wQBO	6	7
	eQBO	9	6
Jan	wQBO	10	7
	eQBO	7	8
Feb	wQBO	9	7
	eQBO	7	8
Mar	wQBO	9	6
	eQBO	8	7

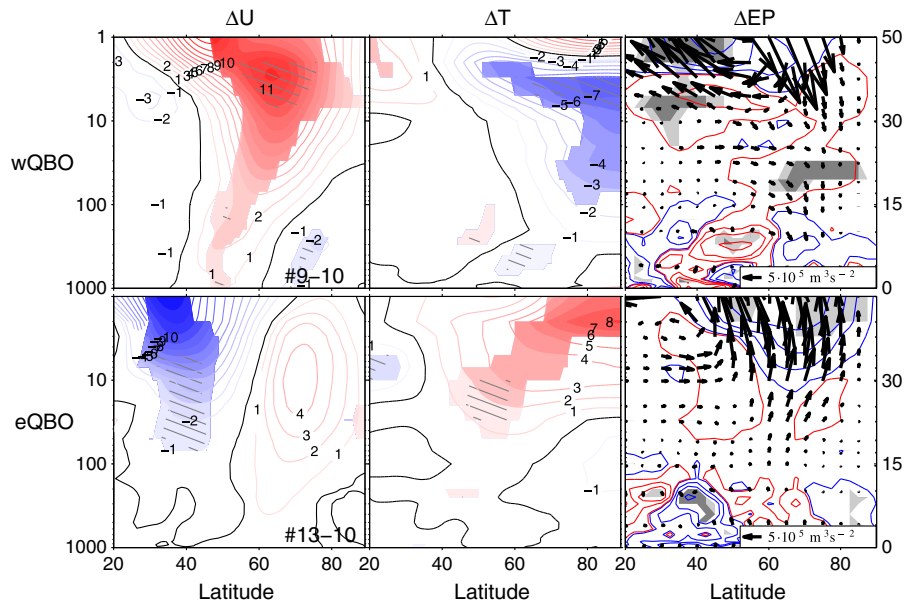
Corresponding to results presented in Figure 3.

irradiance cycle does. To examine whether or not the stratospheric QBO modulates the geomagnetic A_p signal, we also analyzed the composite differences according to the QBO for each calendar month. The large bias toward wQBO for LA_p in November significantly reduces the sample size in the eQBO group, making it very hard to establish statistical significance. A possibility for a QBO modulation of the geomagnetic signal may occur in December, for which the HA_p-LA_p composite differences for wQBO and eQBO are shown in Figure 6. Under wQBO (top), the geomagnetic signal is marked by a strengthening of the stratospheric polar vortex with less wave breaking in the high-latitude lower to midstratosphere as more waves propagate into the low latitude upper stratosphere. Under eQBO (bottom), however, the signal is characterized by a more disturbed polar vortex at its equatorward side as a result of more wave breaking in the upper stratosphere.

[32] In order to illustrate the modulating effect, the QBO has on the early winter geomagnetic signal in wave breaking as well as possible contamination from the ENSO, major volcano eruptions, and the major SSWs, Figure 7 presents all the December monthly mean anomalies for the EP flux

divergence at 35°N – 70°N and 50–70 hPa as a function of the normalized October–December A_p . In this region, the EP flux divergence is a useful measure of the wave-mean flow interaction, especially for the amount of planetary waves propagating from the lower atmosphere into the upper stratosphere. A positive relationship between A_p and EP flux divergence implies more planetary waves propagating from the lower stratosphere into the upper stratosphere and above during high geomagnetic conditions. When all the December data were included, the correlation between A_p and EP flux divergence is only 0.02 (left-hand panel of Figure 7). It is evident that SSWs were more likely to be associated with the eQBO, consistent with the previous findings [see, e.g., Holton and Tan, 1980]. Neither major ENSO events nor major volcano eruptions were able to induce any significant relationship between A_p and EP flux divergence. However, a significant positive correlation appears when only the wQBO years are included (right-hand panel, $r = 0.43$), suggesting that more planetary waves propagate into the upper stratosphere and beyond with less planetary wave breaking (divergence) in the midlatitude lower stratosphere under wQBO and high geomagnetic activity.

[33] ENSO has been shown to have a significant effect on the Northern Hemisphere winter polar vortex. Both observational and modeling studies have shown that the warm phase of ENSO (WENSO) leads to a warmer polar stratosphere [see, e.g., Sassi *et al.*, 2004]. To examine the possible bias due to a large temperature effect caused by the major El Niño events, we repeated our earlier analysis but with the major ENSO affected years (1972–1973, 1982–1983, and 1997–1998) excluded. Quantitatively similar results to Figures 3 and 4 were obtained, suggesting that the major El Niño events do not alter the geomagnetic signature significantly. It also can be seen from Figure 7 that the ENSO years (large squares) do not dominate the relationship between A_p and EP flux divergence in December. The same holds for the other months. Therefore, ENSO has a negligible effect on the A_p signature.

**Figure 6.** December results in the wQBO phase (top) and the eQBO phase (bottom) for All SC years.

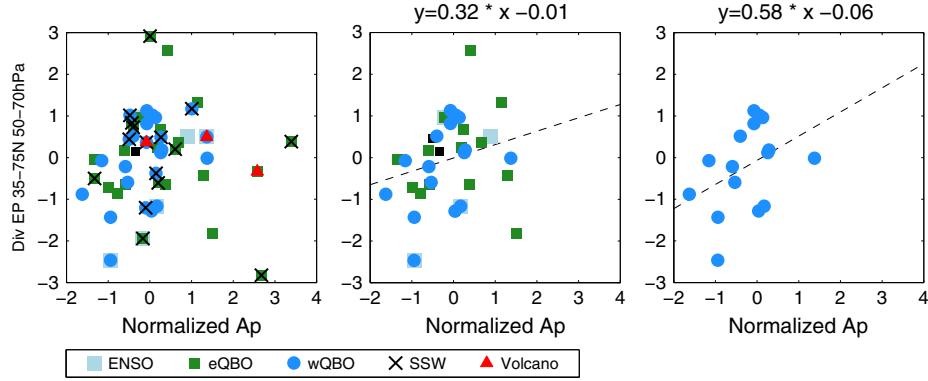


Figure 7. December EP flux divergence anomaly at (35°N – 70°N , 50–70 hPa) as a function of the normalized October–December mean A_p . Major ENSO years, eQBO and wQBO phases, major SSW years, and volcanic eruption years have been indicated with color coding as follows: ENSO (gray square), eQBO (green square), wQBO (blue circle), SSW (black cross), and volcano (red triangle). All other years are shown as black squares. The second panel shows the distribution of the data after SSW and volcanic years are removed. A linear fit to the data points has been added to aid the eye (dashed line). The polynomials for the linear fit are given in the title. The last column further shows the wQBO years only, with SSW and volcanic years removed, and a linear fit to the data points.

[34] Major volcanic eruptions during the ERA period took place during years 1962, 1982, and 1991. We repeated the analysis by excluding the data from the winters following the eruptions, e.g., for the Pinatubo eruption in 1991 we completely exclude the winter 1991–1992, but this did not significantly affect the results (not shown). This can also be demonstrated by looking at the individual case of December in Figure 7, which shows the scatter of the volcanic years (red triangles) for regions where significant EP flux divergence differences were observed between HA_p and LA_p years. For the EP flux divergence, the volcanic years represent both positive and negative anomalies in both A_p and the EP flux divergence but do not generally represent the extreme values. Thus, our analysis regarding inclusion or exclusion of the data affected by the major volcanic eruptions showed no obvious bias on the NH winter geomagnetic signal.

4. Discussion

[35] Our analysis of the ERA data suggests that geomagnetic activity (as measured by the A_p index) can drive significant changes in NH wintertime stratospheric dynamics. The most significant signal is marked by a strengthening of the winds at the poleward edge of the stratospheric vortex and weakening of the wind at the equatorward side of the vortex. The signal first appears in December and propagates poleward and downward over the course of the winter.

[36] When significant responses in the zonal mean zonal wind and temperature were observed, dynamically consistent changes of EP flux and EP flux divergence were also detected. Our analysis of the EP flux anomalies suggests that more planetary waves are refracted equatorward when the geomagnetic A_p index is higher than average. The most significant wave refraction occurs primarily in the upper stratosphere, accompanied by EP flux convergence at low latitudes and EP flux divergence at high latitudes. Similar to the signals in zonal mean zonal wind and temperature, these effects

on EP flux and its divergence propagate poleward following the movement of the polar vortex. As a whole, our analysis confirms that dynamical interaction between the mean flow and planetary waves in the stratosphere play an important role in transferring the geomagnetic activity induced effects poleward, downward, and into the troposphere.

[37] Variations in solar ultraviolet (UV) irradiance that take place over the 11 year solar cycle are known to affect the upper stratosphere, where UV absorption by ozone takes place [Gray *et al.*, 2010]. Increased UV irradiance heats the equatorial upper stratosphere via both direct heating and additional heating from the UV absorption by enhanced stratospheric O_3 [see, e.g., Frame and Gray, 2010]. As such, solar UV and its interaction with stratospheric ozone preconditions the stratosphere background winds for dynamical responses to geomagnetic perturbations. We found that the most significant geomagnetic signature was mainly associated with HS conditions during NH winter. Under HS conditions, equatorward wave refraction started as early as November, intensified during December–February, and became weaker only in March. Under LS conditions, similar wave refraction was observed only in November–January when the stratospheric vortex is the strongest.

[38] Based on our analysis of EP flux and its divergence and the wind and temperature responses, we provide the following explanation for the geomagnetic signal observed in NH winter. The analysis of the EP flux shows that planetary wave activity is modulated by geomagnetic activity. During NH winter when the stratospheric polar vortex is present, the anomalous planetary wave activity interacts with the vortex mainly through wave refraction in the upper stratosphere and when the vortex is relatively strong. This is because planetary waves can only propagate through weak westerly winds. Wave energy is trapped or reflected in regions where the zonal winds are easterly or are large and westerly [Charney and Drazin, 1961]. Under HS conditions, enhanced solar UV and ozone interaction warming the low latitude upper stratosphere leads to an enhanced equator-to-

pole temperature gradient that in turn strengthens the polar vortex. The strengthened polar vortex increases wave refraction away from the high latitudes. This is probably why the geomagnetic A_p signature is largely associated with the HS condition.

[39] Using the same principle, the opposite geomagnetic A_p signals under wQBO and eQBO in December can also be explained through changes in dynamics. Again, as planetary waves can only propagate through weak westerly winds, wave refraction is more likely to occur when the polar vortex is strong. During early winter (November–December), strong westerly winds are typically centered around 1–5 hPa and 35°N–45°N (Figure 2). Under wQBO conditions, the stratospheric polar vortex is known to be stronger than average, while eQBO conditions lead to the vortex being noticeably weaker and warmer [Holton and Tan, 1980], although the exact mechanisms leading to the vortex strength modulation are still somewhat unclear [Garfinkel et al., 2012]. The strengthened polar vortex under wQBO preconditions the upper stratosphere to enable more planetary waves to be refracted equatorward in a similar way as under HS conditions. As a result, the poleward side of the polar vortex is less disturbed. The waves refracted equatorward will eventually become unstable and break at 5 hPa and above, leading to more disturbed winds at the equatorward side of the vortex. Therefore, the solar UV and stratospheric QBO have a key role in affecting the latitude and altitude regions where planetary waves propagate and break and thus modulating the response to geomagnetic forcing. The reason why the strongest QBO modulating effect of the geomagnetic signal was observed in early winter is that the QBO-wave-vortex interaction is at its strongest in early winter rather than late winter [Lu et al., 2008c].

[40] Our analysis of EP flux and its divergence indicated that the tropospheric jets may also respond to geomagnetic perturbations. The most noteworthy signal is the EP flux divergence at 50°N–60°N and EP flux convergence at 35°N–45°N in January–March under HS condition and in December under wQBO condition. These kinds of anomalies in the EP flux divergence are often associated with a poleward shift of the eddy-driven jet or a weakening of the tropospheric subtropical jet. Although it is not clear from our EP flux analysis whether or not a change of synoptic waves is involved to cause such a change in tropospheric jet location or strength, the signals themselves are consistent with stratospheric influence on the troposphere under the condition of strong vortex and a positive NAM [Thompson and Wallace, 2001; Kushner and Polvani, 2004; Kunz et al., 2009].

[41] The All SC HA_p and HS- HA_p stratospheric polar temperature response, with a warming signal in the upper stratosphere and a cooling signal below at high latitudes in January–February, is very similar to those predicted by Baumgaertner et al. [2011] and Semeniuk et al. [2011] as a seasonal mean temperature response to enhanced EPP. Based on earlier work by others, Baumgaertner et al. [2011] suggested that the warming signal would be a result in decrease in ozone radiative cooling as a response to ozone depletion, and the cooling signal might arise from dynamical heating due to slowing down of the meridional Brewer–Dobson circulation. Such a reduction would be associated with less upward EP flux and more waves reflecting toward

the equator [see Lu et al., 2008b, and references therein]. As discussed above, this is now confirmed by our EP flux results.

5. Conclusions

[42] Our aim in this study was to investigate the wave-mean flow interaction as a part of the mechanism linking geomagnetic forcing to changes in stratospheric and tropospheric dynamics. One of the key goals was to help understand the links between the well understood chemical responses to energetic particle precipitation and changes in stratospheric and tropospheric dynamical variables as a result of geomagnetic activity.

[43] Using the ECMWF ERA meteorological re-analysis data, we found that for high geomagnetic activity levels the stratospheric polar vortex becomes stronger, with more planetary waves being refracted equatorward, with the signals appearing in December and continuing until March, and with poleward propagation of the signals with time.

[44] For high geomagnetic activity levels, the dynamical signals are marked by the following:

[45] (1) Reduced upward propagation of waves into the stratosphere in early winter, followed by

[46] (2) Enhanced equatorward reflection of waves from the polar vortex edge,

[47] (3) Warming of the polar upper stratosphere and cooling below, starting in December–January and continuing into March,

[48] (4) Descent of the warming signal from January to March,

[49] (5) Anomalously strong polar vortex in late winter, as measured by changes in zonal mean zonal winds, leading to positive Northern Annular Mode anomalies.

[50] Overall, these results indicate that the geomagnetic effect on planetary wave propagation tends to take place when the stratosphere background flow is relatively stable or when the polar vortex is stronger and less disturbed in early winter (under high solar irradiance cycle or wQBO conditions). Under those conditions, the EPP-generated NO_x would more likely be maintained inside the polar vortex and even transported downward from the mesosphere-lower thermosphere region to interact indirectly with stratospheric dynamics through wave-mean flow interaction. The reduced planetary wave breaking in the lower stratosphere results in more planetary waves propagating into the low latitude upper stratosphere, which then results in the dynamic responses seen later during the winter (January–March).

[51] These results confirm the previous hypothesis of Lu et al. [2008b] regarding the role of dynamics in coupling geomagnetic activity levels and stratospheric changes and supports the suggestion of Baumgaertner et al. [2011] about the dynamical coupling mechanism connecting EPP- NO_x induced ozone loss, polar stratospheric temperatures, and the modulation of the Northern Annular Mode. These results provide a significant step in understanding the chemical-dynamical coupling mechanisms connecting geomagnetic activity/EPP and tropospheric variations found in previous studies [Rozanov et al., 2005; Seppälä et al., 2009]. While our analysis is based on the longest available re-analysis data set (~50 years), the limited amount of data available will always leave some level of uncertainty on the

statistical results. Therefore, more work, including modeling studies where external forcing can be controlled and long simulations can be performed to reduce effects from internal variability, is needed to fully understand the solar wind-lower atmosphere coupling.

Appendix A.

[52] We applied the Student's t test to our results as a statistical significance test. In order to check the robustness of Student's t test results, we chose to also apply a

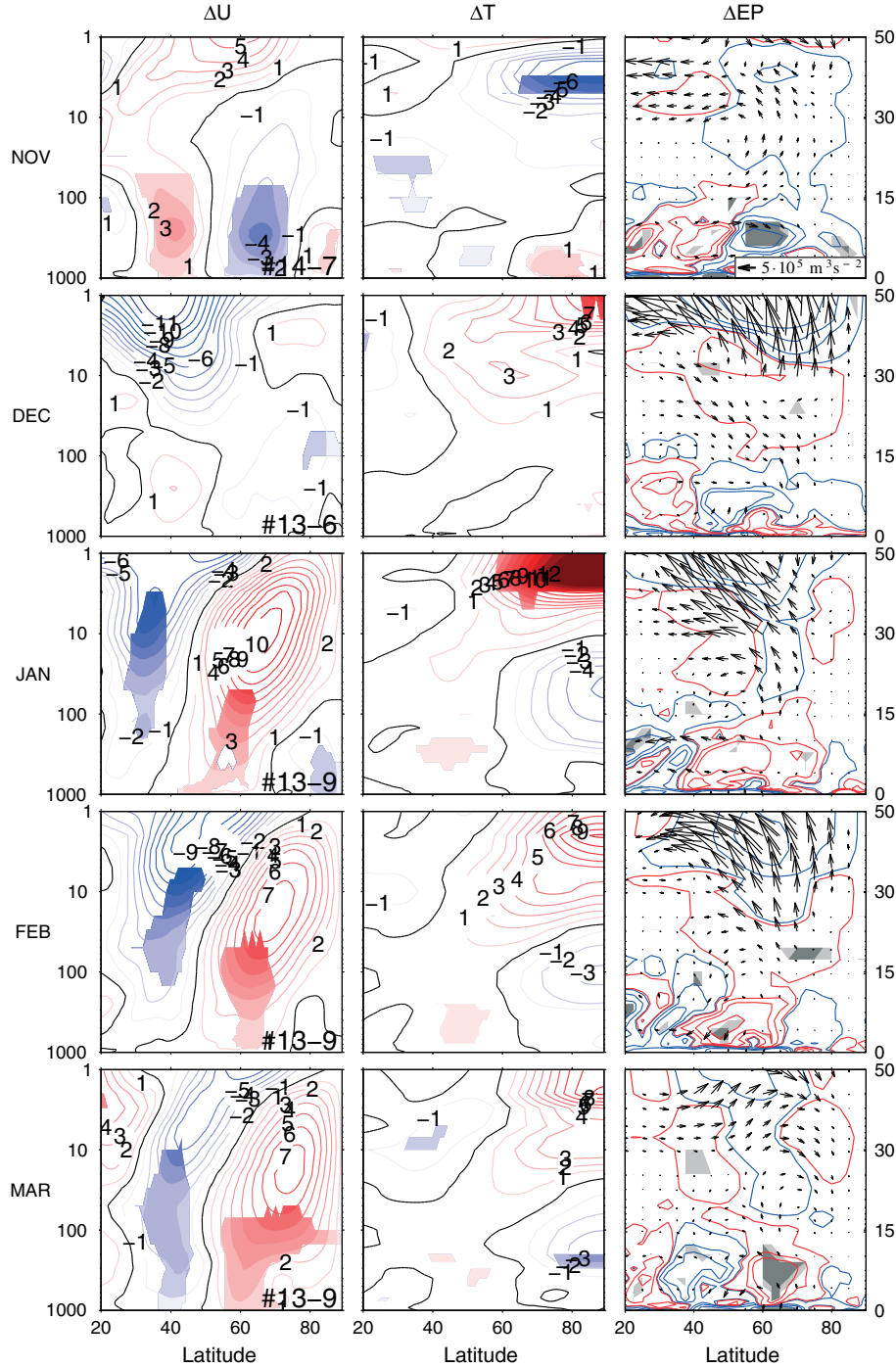


Figure A1. Monthly diagnostics for HS at latitudes 20°N–90°N and pressure levels 1–1000 hPa (approximate altitude [km] shown on right) with statistical significance calculated with the random permutation test. Columns from left to right: zonal mean U difference ΔU , $HA_p - LA_p$; zonal mean T difference ΔT , $HA_p - LA_p$; and the difference in EP flux and divergence ΔEP , $HA_p - LA_p$. The $\geq 90\%$ significance levels are indicated for ΔU and ΔT as in Figure 4. Both $\geq 90\%$ and $\geq 95\%$ levels are presented for the EP flux divergence as in Figure 4. The EP fluxes were scaled according to *Bracegirdle* [2011], and the EP flux reference vector ($5 \times 10^5 \text{ m}^3 \text{ s}^{-2}$) is given in the top EP panels.

secondary statistical test to a part of the analysis. We chose to use the random permutation test with 10,000 repetitions. This test is recommended for testing if the difference of two groups is statistically significant (personal communication, Dr. M. Laine, FMI, 2012).

[53] The random permutation test was performed in the standard way by taking the data under investigation and randomly assigning the individual data points to two groups, which respectively correspond in size to the two groups under investigation. For example, when calculating the composite differences $HA_p - LA_p$, group A will correspond in size to HA_p and group B to LA_p , but individual points are assigned to A and B from the $[HA_p, LA_p]$ pool in random. The composite difference $A - B$ is then calculated. This process is repeated a number of times to find the range outside which the $HA_p - LA_p$ difference is significant at the $\geq 90\%$ or $\geq 95\%$ level.

[54] Figure A1 presents the results for the HS case. The ΔU , ΔT , and ΔEP results are identical to those presented in Figure 4, but the filled-in regions now correspond to those returned by the random permutation test. We calculated the $\geq 90\%$ levels for ΔU and ΔT , and both $\geq 90\%$ and $\geq 95\%$ levels for the ΔEP . As can be seen, contrasting Figures 4 and A1, the results from the two statistical significance tests are very consistent.

[55] Based on the results being very similar from both test, and the fact that the random permutation test is significantly more time-consuming computationally ($> 10\times$) than the t test, there is no extra benefit in applying the random permutation test for the whole ERA data set. Rather this test gives an indication of how well the t test performs.

[56] **Acknowledgments.** We thank the Alfred-Wegener Institute for Polar and Marine Research for making the ERA-40 and ERA Interim EP fluxes available. A.S. would like to thank Drs A. Orr and T. Braccgirdle at BAS for guidance in the EP analysis, and Drs M. Laine and J. Tamminen from FMI for helpful discussions and advice on statistical significance testing. Part of the work of A.S. was done during a visit to the British Antarctic Survey and was funded by the FP7 project FP7-PEOPLE-IEF-2008/237461. Work of A.S. at FMI was funded by the Finnish Academy projects CLASP (258165, 265005) and SAARA (128261). H.L. was funded by the grant NE/I010173/1 of the UK Natural Environment Research Council (NERC). C.J.R. was supported by the New Zealand Marsden Fund.

References

- Andersson, M. E., P. T. Verronen, S. Wang, C. J. Rodger, M. A. Clilverd, and B. R. Carson (2012), Precipitating radiation belt electrons and enhancements of mesospheric hydroxyl during 2004–2009, *J. Geophys. Res.*, **117**, D09304, doi:10.1029/2011JD017246.
- Andrews, D. G., J. R. Holton, and C. B. Leovy (1987), *Middle Atmosphere Dynamics*, Academic Press, London.
- Baldwin, M. P., and T. J. Dunkerton (2001), Stratospheric harbingers of anomalous weather regimes, *Science*, **294**(5542), 581.
- Baumgaertner, A. J. G., P. Jöckel, and C. Brühl (2009), Energetic particle precipitation in ECHAM5/MESSy1–Part 1: Downward transport of upper atmospheric NO_x produced by low energy electrons, *Atmos. Chem. Phys.*, **9**, 2729–2740.
- Baumgaertner, A. J. G., A. Seppälä, P. Joeckel, and M. A. Clilverd (2011), Geomagnetic activity related NO_x enhancements and polar surface air temperature variability in a chemistry climate model: Modulation of the NAM index, *Atmos. Chem. Phys.*, **11**(9), 4521–4531, doi:10.5194/acp-11-4521-2011.
- Braccgirdle, T. J. (2011), The seasonal cycle of stratosphere-troposphere coupling at southern high latitudes associated with the semi-annual oscillation in sea-level pressure, *Clim. Dyn.*, doi:10.1007/s00382-011-1014-4, (to appear in print).
- Charlton, A. J., and L. M. Polvani (2007), A new look at stratospheric sudden warmings. Part I: Climatology and modeling benchmarks, *J. Climate*, **20**(3), 449–469, doi:10.1175/JCLI3996.1.
- Charney, J. G., and P. G. Drazin (1961), Propagation of planetary-scale disturbances from the lower into the upper atmosphere, *J. Geophys. Res.*, **66**(1), 83, doi:10.1029/JZ066i001p00083.
- Cohen, J., D. Salstein, and K. Saito (2002), A dynamical framework to understand and predict the major Northern Hemisphere mode, *Geophys. Res. Lett.*, **29**(10), 1412, doi:10.1029/2001GL014117.
- Frame, T. H. A., and L. J. Gray (2010), The 11-Yr solar cycle in ERA-40 Data: An update to 2008, *J. Climate*, **23**(8), 2213–2222, doi:10.1175/2009JCLI3150.1.
- Garfinkel, C. I., T. Shaw, D. L. Hartmann, and D. W. Waugh (2012), Does the Holton–Tan Mechanism explain how the quasi-biennial oscillation modulates the Arctic Polar Vortex? *J. Atmos. Sci.*, **69**(5), 1713–1733.
- Gray, L. J., et al. (2010), Solar influences on climate, *Rev. Geophys.*, **48**(4), RG4001, doi:10.1029/2009RG000282.
- Holton, J. R., and H. C. Tan (1980), The influence of the equatorial quasi-biennial oscillation on the global circulation at 50 mb, *J. Atmos. Sci.*, **37**(10), 2200–2208.
- Holton, J. R., P. H. Haynes, M. McIntyre, A. R. Douglass, R. Rood, and L. Pfister (1995), Stratosphere–troposphere exchange, *Rev. Geophys.*, **33**(4), 403–439.
- Kunz, T., K. Fraedrich, and F. Lunkeit (2009), Impact of synoptic-scale wave breaking on the NAO and its connection with the stratosphere in ERA-40, *J. Climate*, **22**(20), 5464–5480, doi:10.1175/2009JCLI2750.1.
- Kushner, P. J., and L. M. Polvani (2004), Stratosphere–troposphere coupling in a relatively simple AGCM: The role of eddies, *J. Climate*, **17**(3), 629–639.
- Kvissel, O. K., Y. J. Orsolini, F. Stordal, I. S. A. Isaksen, and M. L. Santee (2012), Formation of stratospheric nitric acid by a hydrated ion cluster reaction: Implications for the effect of energetic particle precipitation on the middle atmosphere, *J. Geophys. Res.*, **117**(D16), D16301, doi:10.1029/2011JD017257.
- Labitzke, K., and M. Kunze (2009), On the remarkable Arctic winter in 2008/2009, *J. Geophys. Res.*, **114**(3), doi:10.1029/2009JD012273.
- Langematz, U. (2000), An estimate of the impact of observed ozone losses on stratospheric temperature, *Geophys. Res. Lett.*, **27**(14), 2077–2080, doi:10.1029/2000GL011440.
- Langematz, U., M. Kunze, K. Krüger, K. Labitzke, and G. Roff (2003), Thermal and dynamical changes of the stratosphere since 1979 and their link to ozone and CO₂ changes, *J. Geophys. Res.*, **108**, 4027, doi:10.1029/2002JD002069.
- Lockwood, M., R. G. Harrison, T. Woollings, and S. K. Solanki (2010), Are cold winters in Europe associated with low solar activity?, *Environ. Res. Lett.*, **5**(2), 4001, doi:10.1088/1748-9326/5/2/024001.
- Lu, H., M. P. Baldwin, L. J. Gray, and M. J. Jarvis (2008c), Decadal-scale changes in the effect of the QBO on the northern stratospheric polar vortex, *J. Geophys. Res.*, **113**(D10), D10114, doi:10.1029/2007JD009647.
- Lu, H., M. A. Clilverd, A. Seppälä, and L. L. Hood (2008a), Geomagnetic perturbations on stratospheric circulation in late winter and spring, *J. Geophys. Res.*, **113**, D16106, doi:10.1029/2007JD008915.
- Lu, H., M. J. Jarvis, and R. Hibbins (2008b), Possible solar wind effect on the northern annular mode and northern hemispheric circulation during winter and spring, *J. Geophys. Res.*, **113**, D23104, doi:10.1029/2008JD010848.
- Lu, H., L. J. Gray, M. P. Baldwin, and M. J. Jarvis (2009), Life cycle of the QBO-modulated 11-year solar cycle signals in the Northern Hemispheric winter, *Q. J. R. Meteorol. Soc.*, **135**(641), 1030–1043, doi:10.1002/qj.419.
- Manney, G. L., M. J. Schwartz, K. Krüger, M. L. Santee, S. Pawson, J. N. Lee, W. H. Daffer, R. A. Fuller, and N. J. Livesey (2009), Aura Microwave Limb Sounder observations of dynamics and transport during the record-breaking 2009 Arctic stratospheric major warming, *Geophys. Res. Lett.*, **36**(12), L12815, doi:10.1029/2009GL038586.
- Palmer, T. (1981), Diagnostic study of a wavenumber-2 stratospheric sudden warming in a transformed Eulerian-mean formalism, *J. Atmos. Sci.*, **38**, 844–855.
- Randall, C. E., V. L. Harvey, C. S. Singleton, S. M. Bailey, P. F. Bernath, M. Codrescu, H. Nakajima, and J. M. Russell III (2007), Energetic particle precipitation effects on the Southern Hemisphere stratosphere in 1992–2005, *J. Geophys. Res.*, **112**, D08308, doi:10.1029/2006JD007696.
- Randall, C. E., et al. (2005), Stratospheric effects of energetic particle precipitation in 2003–2004, *Geophys. Res. Lett.*, **32**, L05802, doi:10.1029/2004GL022003.
- Rozanov, E., L. Callis, M. Schlesinger, F. Yang, N. Andronova, and V. Zubov (2005), Atmospheric response to NQy source due to energetic electron precipitation, *Geophys. Res. Lett.*, **32**, L14811, doi:10.1029/2005GL023041.
- Salmi, S.-M., P. T. Verronen, L. Thölix, E. Kyrölä, L. Backman, A. Y. Karpechko, and A. Seppälä (2011), Mesosphere-to-stratosphere descent of odd nitrogen in February–March 2009 after sudden stratospheric warming, *Atmos. Chem. Phys.*, **11**(10), 4645–4655, doi:10.5194/acp-11-4645-2011.

- Sassi, F., D. E. Kinnison, B. A. Boville, R. R. Garcia, and R. Roble (2004), Effect of El Niño–Southern Oscillation on the dynamical, thermal, and chemical structure of the middle atmosphere, *J. Geophys. Res.*, **109**(D17), D17108, doi:10.1029/2003JD004434.
- Semeniuk, K., V. I. Fomichev, J. C. McConnell, C. Fu, S. M. L. Melo, and I. G. Usoskin (2011), Middle atmosphere response to the solar cycle in irradiance and ionizing particle precipitation, *Atmos. Chem. Phys.*, **11**(10), 5045–5077, doi:10.5194/acp-11-5045-2011.
- Seppälä, A., P. T. Verronen, M. A. Clilverd, C. E. Randall, J. Tamminen, V. Sofieva, L. Backman, and E. Kyrölä (2007), Arctic and Antarctic polar winter NO_x and energetic particle precipitation in 2002–2006, *Geophys. Res. Lett.*, **34**, L12810, doi:10.1029/2007GL029733.
- Seppälä, A., C. E. Randall, M. A. Clilverd, E. Rozanov, and C. J. Rodger (2009), Geomagnetic activity and polar surface air temperature variability, *J. Geophys. Res.*, **114**, A10312, doi:10.1029/2008JA014029.
- Sinnhuber, M., S. Kazeminejad, and J. M. Wissing (2011), Interannual variation of NO_x from the lower thermosphere to the upper stratosphere in the years 1991–2005, *J. Geophys. Res.*, **116**, A02312, doi:10.1029/2010JA015825.
- Siskind, D. E., G. E. Nedoluha, C. E. Randall, M. Fromm, and J. M. Russell III (2000), An assessment of Southern Hemisphere stratospheric NO_x enhancements due to transport from the upper atmosphere, *Geophys. Res. Lett.*, **27**, 329–332, doi:10.1029/1999GL010940.
- Thompson, D. W. J., and J. M. Wallace (1998), The arctic oscillation signature in the wintertime geopotential height and temperature fields, *Geophys. Res. Lett.*, **25**, 1297–1300.
- Thompson, D. W. J., and J. M. Wallace (2001), Regional climate impacts of the Northern Hemisphere annular mode, *Science*, **293**(5527), 85.
- Uppala, S. M., et al. (2005), The ERA-40 re-analysis, *Q.J.R. Meteorol. Soc.*, **131**(612), 2961–3012, doi:10.1256/qj.04.176.
- Verronen, P. T., M. L. Santee, G. L. Manney, R. Lehmann, S.-M. Salmi, and A. Seppälä (2011), Nitric acid enhancements in the mesosphere during the January 2005 and December 2006 solar proton events, *J. Geophys. Res.*, **116**, D17301, doi:10.1029/2011JD016075.